

THERMAL EVOLUTION OF TERRESTRIAL EXOPLANETS

—SYSTEM EARTH MODELLING MASTERS THESIS

Supervisor: Dr. A. P. van den Berg
Institute of Earth Sciences

Utrecht University

Yue Zhao

August 30, 2011

Abstract

The recent rapid development in the detection and characterisation of exoplanets (planets outside the Solar System) call for a systematic comparison of their thermal state and planetary history under different internal conditions. Previous studies suggest that the initial condition of the Earth's thermal history is 'forgotten' relatively early in its history and therefore does not contribute to the Earth's current thermal state. This does not hold true for large terrestrial exoplanets based on similar calculations for larger planetary sizes. In this study we use a steady state temperature profile just below the solidus as the initial condition. A series of numerical modelling experiments are performed to investigate the effects of planetary size, surface temperature, depth-dependent viscosity profiles and the core mass ratio of the planet. Both a parameterised modelling approach and a dynamical approach are applied to thermal convection models in a hierarchy of complexity. Thermal equilibrium models are performed to study the effects of planetary internal conditions on steady state temperatures and thus suitable initial conditions for the investigation of subsolidus thermal convection, while thermal evolutionary experiments study the effects of these parameters on exoplanetary thermal history.

We find that larger planets in general cool slower from an initial hot state, due to larger total internal production of heat and relatively low surface-to-volume ratio. In their early history, planets with a smaller core are more likely to be in a thermal regime of periodic melting than those of an equal mass and larger core, their subsolidus cooling being accordingly delayed. This is a combined effect of larger planetary size, rapid decrease of gravitational acceleration with depth, and relatively low melting temperatures. "Super-plumes" are observed in planets without a metal core, which efficiently transport hot materials to the surface and thereby decrease the planet's internal thermal gradient. Depth-dependent viscosity profiles calculated from an Arrhenius type of formulation are found to suppress surface thermal instabilities and mobilise the low-viscosity zones in the upper part and the bottom of the mantle layer. When the depth-dependence of viscosity is considered, convective motion is propelled by warm upwellings close to the core mantle boundary while the surface is characterised by a thick boundary layer of stable conduction. This in turn changes the internal thermal structure of the planet and increases steady state temperatures.

Contents

1	Introduction	1
2	Planetary thermal history	3
2.1	The initial condition of thermal evolution	3
2.1.1	Effects of the initial condition on planetary thermal history	3
2.1.2	Using steady state temperatures as the initial condition	4
2.2	The rate of cooling and planetary thermal structure	5
3	Parameterised models	5
3.1	Governing equations and numerical modelling methods	6
3.2	Modelling the effect of exoplanet mass	7
3.3	Exoplanet surface temperature	8
3.4	Comparison with dynamical models	10
4	Dynamical models	11
4.1	Governing equations	11
4.2	Numerical techniques and resolution	11
4.3	Exoplanets with an Earth-like core-mass fraction	12
4.3.1	Modelling the effects of depth-dependent viscosity	12
4.3.2	Model description	13
4.3.3	Results	15
4.4	Core-less exoplanets	16
4.4.1	The internal conditions of core-less planets	16
4.4.2	Modelling the steady state temperature in core-less planets	18
4.4.3	Thermal evolution of core-less planets	20
4.4.4	Super-plumes	22
5	Discussions and conclusion	24
6	Acknowledgement	26
A	Depth-dependent viscosity	29
B	The density, adiabatic temperature, and solidus profiles of core-less dynamical models	31

List of Figures

1	Thermal evolution of planets with different masses	9
2	Thermal evolution of planets with different surface temperatures	9
3	Comparison between parameterised convection models and dynamical models for planet with Earth-like core-mass ratio	10
4	Meshes used in two series of dynamical models.	12
5	Depth-dependent viscosity profile and initial temperature profile of core planets . . .	13
6	Time series of temperature and heat flow values of A1 and A2	16
7	Temperature and velocity profiles of A1 and A2	17
8	2-D temperature plots of A1 and A2	17
9	Time series of temperature and heat flow values of A3 and A4	18
10	Steady state temperatures of core-less planets	19
11	The solidus of core-less planets and the adiabatic temperature profile that corresponds to 50% melting	19
12	Initial temperature profile of core-less planets	21
13	Time series of temperature and heat flow in B1 and B2	21
14	Times series of the average velocity amplitude in B1 and B2	21
15	2-D temperature plots of B1 and B2	22
16	2-D temperature plots of a super-plume in core-less planets	23
17	Time series of heat flow and velocity and temperature and velocity profiles during a super-plume event	24
18	Depth-dependent viscosity profiles. <i>expo</i> and <i>arrh</i> in the legend denote the exponential viscosity model and the Arrhenius model, respectively. For exponential models, $\Delta\eta_T$ and $\Delta\eta_P$ are listed. For Arrhenius models, the viscosity prefactor is indicated. .	30

List of Tables

1	Explanation of parameters used in parameterised model equations and model set-up (Table 2).	7
2	Models investigating effects of planetary mass.	8
3	Parameterised convection models investigating effects of surface temperature, to be updated.	10
4	Dynamical models of planets with an Earth-like core-mass fraction	14
5	Parameters used in dynamical models	15
6	Model set-up of B1 and B2	23
7	Parameters used in dynamical models with Earth-like core mass fraction.	30

1 Introduction

An extra-solar planet (exoplanet) is a planet orbiting a star that is outside the Solar System. The discovery of a planetary system around PSR 1257+12 (Wolszczan and Frail) in 1992 confirmed the existence of terrestrial planets outside the Solar System, and offered new hope for a habitable home for future mankind. Up to August 2011, more than 500 extrasolar planets have been discovered (JPL, 2011). The majority of them are detected by the radial velocity method, and most of these have masses larger than $10 M_{\oplus}$ (10 times the Earth’s mass). Such planets are expected to be gaseous, like Jupiter in our Solar System. More than 30 (NStED, 2011) of these exoplanets have masses less than $10 M_{\oplus}$, which are most likely terrestrial and are defined as super-Earths. The CoRoT and Kepler space missions (launched in 2006 and 2009, respectively) are particularly capable of detecting super-Earths. A list of over 1200 planet candidates were announced by the Kepler Science Team in February 2011 for confirmation by independent observations (Borucki et al., 2011). Moreover, observations from spectral instruments included in the James Webb Space Telescope (JWST) enable us to characterise surface and atmospheric properties of transiting exoplanets. Stellar spectrum analysis during transits can shed light on the chemical composition of the planet’s upper atmosphere, while increased light intensity during secondary eclipse may indicate the temperature of the planet.

The recent rapid development in the detection and characterisation of exoplanets has received much international attention (Valencia et al., 2006; O’Neill and Lenardic, 2007; van den Berg et al., 2005). Such developments offer opportunities for comparative planetological studies, in which knowledge of exoplanetary interiors is obtained by a systematic comparison of internal structure and thermal history under different planetary conditions. Due to the lack of direct observations, at the moment numerical modelling is the principle tool of investigation for such planetary comparisons. Aims of exoplanetary interior modelling studies include investigations of the convective style (with consequences of plate tectonics and surface features; van Thienen et al., 2004; O’Neill and Lenardic, 2007; Valencia et al., 2007), mass–radius relation (Fortney et al., 2007; Sotin et al., 2007; Seager et al., 2007), and the internal structure of a terrestrial exoplanet (Valencia et al., 2006; Valencia et al., 2010). All these phenomena are linked by the thermal history of the planet. Effects of the internal conditions expected on super-Earths on a range of temperature- and pressure-dependent parameters relevant to planetary thermal evolution have been investigated (van den Berg et al., 2010; Tackley et al., 2011).

In this study I will only focus on super-Earths, the terrestrial exoplanets. For convenience, ‘exoplanet’ in the subsequent text specifically refers to terrestrial exoplanets. Since substantial heating and possible extensive melting of the mantle are expected to have happened only in the Earth’s early history, most thermal evolution studies of the Earth’s mantle focus on subsolidus convection. Previous studies of the Earth’s thermal history arrived at the conclusion that, in the forward integration of time series, the initial thermal condition is ‘forgotten’ relatively early in Earth’s history. This implies that the prescription of the initial condition, though involving much uncertainty, does not have much influence on the Earth’s present thermal state. In Section 2.1.1, I will demonstrate that this does not necessarily hold true for planets with larger masses. This research project will first investigate whether the initial condition influences the thermal history of large exoplanets, and if so, what would be a reasonable choice of the initial condition.

It will then explore the extent to which various exoplanetary internal conditions affect the speed

and style of the thermal evolution in planetary interiors. In particular, the research focuses on the effects of the physical properties that vary with planetary size and are strongly associated with the dynamics of thermal evolution. Super-Earths have masses up to $10 M_{\oplus}$. This allows for a wide range of possible internal structures and potentially very high temperature and pressure internal conditions. If a planet with $8 M_{\oplus}$ is purely made of iron (giant core), taking an average density of $13 \times 10^3 \text{ kg/m}^3$, the planet would have a radius of 9574 km, only 1.5 times that of the Earth. The pressure at the centre of such a planet may reach as high as 2.16 TPa. If a planet of equal mass is only made of silicates with an average density $= 5 \times 10^3 \text{ kg/m}^3$, it would have a radius of more than twice that of the Earth, but only reaching 0.61 TPa at its centre. At a surface potential temperature of 1600 K, an adiabatic extrapolation based on a uniform density profile gives this silicate planet a temperature of 4669 K at its centre. The size and structure of a planet determine the temperature and pressure conditions in its interior and therefore dictate the range of temperature- and/or pressure-dependent parameters that control of style and rate of exoplanetary thermal evolution.

In summary, this research project attempts to address the following two general questions:

1. How do the different internal conditions (temperature, pressure, geometry, etc.) of an exoplanet lead to differences in their thermal state and planetary history?
2. What is a suitable initial condition for the study of exoplanetary thermal history?

In the numerical modelling of hypothetical exoplanets, it is often assumed that the exoplanet has a similar inner structure as the Earth (van den Berg et al., 2010; O'Neill et al., 2007). While this is very useful in investigating the effects of some parameters as they scale with, for instance, the size of the planet, the effects of different internal structure have not been systematically tested. Even within our own solar system, a wide range of planetary interiors can be found. Jupiter's moon Europa is believed to have an icy crust, an oceanic layer, silicate mantle, and an inner iron core. Mercury has a core volume fraction more than twice that of the Earth. One effective way of modelling the effects of the inner structure is to vary the size of the planet's core. The core size does not only change the geometry of the mantle domain, where convective thermal transportation takes place, but also strongly affects the gravity profile of the whole planet. This would in turn affect a range of pressure-dependent parameters. Modelling experiments are performed in this project to investigate the effects of planetary size and core mass ratio on the planet's thermal evolution.

Viscosity is a crucial parameter in the modelling of mantle convection, and is directly related to the convective vigour. Early literature often parameterises viscosity in an exponential relation with temperature (Davies, 1980; Valencia, 2006). This equation only takes the temperature dependence of rheology into account and is useful in simple parameterised models (as in Section 3) when a global average viscosity is coupled with the average temperature. Viscosity decreases with increasing temperature, but geophysical studies suggest that the lower mantle has a higher viscosity than the upper mantle, despite its higher temperature. This is due to an increased pressure at depth. In the interior of large exoplanets, where pressure conditions may reach 1 TPa (van den Berg et al., 2010), the depth dependence of viscosity may be stronger. It is therefore important to investigate the effects of depth-dependent viscosity models on exoplanetary thermal evolution. An Arrhenius type of formulation, which expresses both temperature and pressure dependence, is used to model viscosity in this study. Especially, effects of the pressure dependence of viscosity is studied. At the same time, the surface temperature of an exoplanet influences the rate of cooling by controlling the

temperature contrast across the surface thermal boundary layer. A wide range of surface temperatures are expected on exoplanets as they have different orbits to their sun and different atmospheric conditions. Therefore the effects of surface temperature on exoplanetary thermal evolution is also investigated.

Two modelling approaches, parameterised models and dynamical models, are applied and compared in this study. A series of modelling experiments are performed with an increasing degree of complexity to investigate effects of planetary size, surface temperature, core mass fraction, and viscosity models. The dynamical modelling approach obtains approximate solutions to the set of partial differential equations (Section 4.1) describing convective motion, using the Finite Element Method. The parameterised approach, on the other hand, assumes a power-law scaling relation between boundary heat flow and the Rayleigh number (Schubert et al., 1979), thereby reducing the problem to a set of ordinary differential equations (Section 3.1). Differences between the two methods lie in sources of uncertainties, numerical techniques, resolution, and the implementation of physical processes. Parameterised models introduce more uncertainties and does not have the spatial resolution of dynamical models. But they are very efficient in terms of computational time and power. They are commonly used in first-order estimations and preliminary tests for models of higher complexity. In this project, knowledge obtained from dynamical models is used in the parameterisation of the parameterised convection models. A comparison between the two modelling approaches is made by applying corresponding parameterization to both (Section 3.4), and tests if the parameterised modelling approach is a justified simplification to the dynamical approach.

To begin with, the following report firstly makes a discussion about planetary thermal history to state some of the problems that this project attempts to solve, and to introduce the common measures of planetary thermal history that can be used in comparing different models. In Section 3, I will introduce the formulation and results of the parameterised models. Dynamical modelling experiments will be presented in Section 3, followed by discussions and conclusions in Section 4. Additional calculations and figures can be found in the Appendix.

2 Planetary thermal history

In this section I will introduce some key concepts relevant to my investigation of planetary thermal history. The problem of the initial condition of the thermal evolution in large exoplanets is investigated. Steady state adiabatic temperatures profiles just below the solidus are suggested to be used as the initial condition. The cooling rate and planetary thermal structure are used as key measures of thermal evolution.

2.1 The initial condition of thermal evolution

2.1.1 Effects of the initial condition on planetary thermal history

The fact that the Earth seems to be a well differentiated body suggest that it has been extensively heated. The sources of primordial heat include residual heat from planetary accretion and early heavy bombardment. The Earth subsequently cools itself by heat loss from its surface. Early researchers that study the thermal history of the Earth found that the initial thermal condition in Earth's early history (the high temperature and the amount of heat stored) is 'forgotten' relatively

early in the Earth’s history. In other words, the cooling of the Earth was so efficient, that the primordial heat makes a negligible contribution to the Earth’s present thermal state. Schubert and his colleagues (Schubert et al., 1979) explored this issue by using a range of initial temperatures as starting points and then making forward integration of the global average temperature to see how it evolves for 4.5 Gyrs, which is about the age of the Earth. They arrived at the conclusion that, for models of the Earth, a difference in 1500 K in the initial temperature resulted in only 32 K difference after 4.5 Gyrs. This difference is larger for planets of different sizes, a phenomenon Schubert et al. also illustrated in the same paper, but they did not make further discussions about it. As I will demonstrate in Section 3.2, planetary size has a strong influence on its cooling rate and may thus influence the contribution of early thermal states to their current thermal state. Moreover, the models of Schubert et al. do not include any internal heating or basal heating (only cooling from primordial heat) and they prescribed a very strong temperature dependence of viscosity. Inclusion of internal heating would delay cooling and therefore delay the time it takes for primordial heat to be transported out of the planet. The high temperature dependence of viscosity also reduces the amount of time needed for a planet to ‘forget’ its initial thermal state, as can be inferred from the analysis of Davies (1980). Davies (1980) and Christensen (1985) introduced the concept of ‘readjustment time’, the time needed for a planet to forget its initial state. Davies calculated such time with the parameterised approach (i.e. power law relation between the heat flow and average temperature). He assumed no heat sources, and an exponential dependence of viscosity on temperature. If the two power-law relations are $Nu = (Ra/Ra_c)^\beta$ and $\eta/\eta_0 = (T/T_0)^{-n}$, then the magnitude of the readjustment time can be written as $t = \tau/(m - 1)$, where $m = 1 + \beta + n\beta$ and $\tau \sim 15$ Gyr for the Earth.

It is therefore important to test the effects of planetary size on the readjustment time when studying the thermal history of planets much larger than the Earth. The Arrhenius viscosity model described in Appendix A corresponds to an n value of 21 in its temperature dependence. Using corresponding exoplanetary temperature and heat flow levels obtained from previous modelling experiments to calculate the τ value, I arrive at an readjustment time of 57 Gyr for an exoplanet of 8 times the Earth’s mass. Simple parameterised models (Section 3.1) of constant viscosity also indicate longer readjustment time for large exoplanets.

2.1.2 Using steady state temperatures as the initial condition

If initial condition is indeed important in the study of planetary thermal history, the next question we ask is what would be a reasonable initial condition. One approach used in planetary thermal evolution studies is to use the steady state temperature of preliminary model runs as the initial condition. The steady state is the thermal state in which internal heat production is balanced by heat flow out of the planet’s boundaries. A planet in a steady state has a constant temperature, which is the steady state temperature. The steady state is a hypothetical state because internal heating would always decay. But it is an important concept as the measure of the thermal condition from which, if the internal heating rate decays, temperature would decrease. All other parameters the same, we can find a one-to-one relationship between internal heating and its steady state temperature. If we start at an initial temperature higher than the steady state temperature that corresponds to the initial internal heating, we have an initial state in which surface heat flow is higher than internal heat production, cooling starts faster than if we start at steady state temperature. Even though it cools faster, it would still give a thermal history of a higher temperature. If we start

at an initial temperature lower than the steady state temperature, an initial heating of the planet would occur. It would give a cooling history with a lower temperature. The combination of initial temperature and initial internal heating can give a unique thermal history. And this thermal history can be characterised by initial temperature and the corresponding steady state temperature of the initial internal heating. Since only subsolidus cooling histories are considered in our modelling experiments, it is also of our interest to compare our initial condition with the melting temperatures in the planet. In Sections 4.3.2 and 4.4.1 I calculate the solidus of exoplanets with an Earth-like core-mass fraction and those with a zero core size. Steady state temperatures that are higher than the melting temperatures are not suitable initial thermal conditions for investigations of subsolidus cooling history, as such temperatures would induce melting. Melting would in turn result in much faster cooling than calculated in subsolidus relations. When we use the highest possible steady state temperature below the solidus, we cannot use an initial condition higher than this steady state temperature, otherwise melting would still occur. If a steady state temperature is used as the initial condition, then it would be a reasonable practice to find a steady state temperature that is below the solidus. This is applied in Sections 4.3.2 and 4.4.1 for thermal history modelling experiments. Effects of planetary size, depth-dependent viscosity, and core-mass ratio on steady state temperatures are also discussed along the way.

2.2 The rate of cooling and planetary thermal structure

If we take the whole planet as the system we study, it has internal heating as a heat source, and heat is lost from the surface to the environment. The rate of cooling therefore depends on the relative relationship between internal heating rate and rate of heat flow at the surface. The abundance and proportions of radioactive elements are estimated based on chondritic meteorites. The estimate of the current internal heating of the earth is $2.55 \times 10^{-12} \text{ W kg}^{-1}$. Based on a fuel mix and the corresponding decay rate, the heating rate 4.5 Gyrs ago, when the Earth was just formed, is about $15 \times 10^{-12} \text{ W kg}^{-1}$. The rate of heat flow at the surface depends on convective vigour in the interior, surface conductivity, and the thermal structure in the surface thermal boundary layer. The thermal history of a planet can influence its current state because it takes time for heat to be transported and temperature to change. Thus the rate of cooling influences the 'readjustment time' of a planet, and is therefore an important measure of thermal history. Effects of various modelling parameters on the cooling rate discussed in evolutionary modelling experiments. The cooling rate of a planet also depends on its thermal structure, which influences convective vigour and style. In the modelling experiments of this study, variations in thermal structures are also observed.

3 Parameterised models

Thermal histories of terrestrial exoplanets are computed in a series of parameterized convection models with increasing degrees of complexity, to study the basic effects of planetary size and surface temperature, and to compare them with corresponding dynamical models. In particular, radius, gravity, and compressibility in a range of super-Earth models of different masses are compared with Earth-like conditions. With higher surface temperature we model the effects of the temperature contrast across the thermal boundary layer. The exoplanets orbiting with different distances around their stars may have different surface temperatures accordingly, though surface temperatures may also be strongly influenced by the atmospheric conditions of the planet. Models of planets with Earth-like core-mass fraction and core-less planets are implemented in both dynamical models and

corresponding parameterised models to gain insight into the differences and similarities between the two modelling approaches.

3.1 Governing equations and numerical modelling methods

Physical processes involved in our models are time-dependent internal heating by the natural decay of unstable radiogenic isotopes, boundary layer conduction and thermal convection. A 3-dimensional spherical geometry of the planet is considered, where volumetric and surface areal values are computed accordingly. Equation 1 describes the conservation of energy in terms of the volumetric average temperature T_m and surface/CMB heat flow densities q_{surf} and q_{cmb} . Taking the spherical shell representing the mantle layer as the studied system, the total rate of change of the thermal energy is the combined effect of heat flow across its boundary surfaces and internal heating. The rate of change of the temperature of the core heat reservoir T_c is described by Equation 2. Equation 3 is the parameterisation of boundary heat flux in terms of the Rayleigh number. The global average temperature is the unknown, and the temperature contrast across the mantle is computed as the difference between the average temperature and the prescribed surface temperature. The thermal coupling between the mantle and the core is considered in all models as shown in Equations 1 and 2.

$$\rho_m c_{p-m} \frac{dT_m}{dt} = \rho_m H(t) - q_{surf}(t) \frac{S_{surf}}{V_m} + q_{cmb}(t) \frac{S_{cmb}}{V_m} \quad (1)$$

$$\rho_c c_{p-c} \frac{dT_c}{dt} = -q_{cmb}(t) \frac{S_{cmb}}{V_c} \quad (2)$$

$$q_{surf} = \frac{k_m \Delta T_{surf}}{D} \left(\frac{Ra}{Ra_c} \right)^\beta \quad (3)$$

$$q_{cmb} = \frac{q_{surf} \Delta T_{cmb}}{\delta \Delta T_{surf}} \quad (4)$$

$$Ra = \frac{\rho_m \alpha g \Delta T_{surf} D^3}{\kappa \eta} \quad (5)$$

Here $q_{surf}(t)$ is the surface heat flow density. q_{cmb} is the CMB heat flow density, which is scaled to q_{surf} by boundary layer thickness in Equation 4, where δ is the ratio of CMB to surface boundary layer thickness. According to my dynamical model results (Figure 7), the boundary layer at CMB is about twice the thickness as the surface boundary. Therefore δ is taken as 2 in the parameterised model calculations. S_{surf} and S_{cmb} are the areas of the planet's surface and CMB, respectively. V_m is the volume of the mantle layer, and V_c that of the core. D is the mantle thickness. Other parameters are explained in Table 1.

In these models, the thermal history of the cooling planet is computed by solving the above ordinary differential equations for the volume averaged mantle and core temperatures. Time series of the average temperature, and other time-dependent parameters, are computed numerically using a second order Runge-Kutta integration scheme. The temperature contrast across the thermal boundary layer, from which the surface heat flux is calculated, is obtained as the difference between the mantle volume average temperature and the surface temperature.

The model formulation corresponds to dynamical convection models including core coupling. Due to the parameterised approach, prescribed density and the unknown temperature are global average values. Free slip and impermeable boundary conditions are implicit in the parameterisation of heat flux in Equation 3 and 4 in terms of the Nusselt number ($Nu = (Ra/Ra_c)^\beta$). Initial average temperature is taken as 3500 K, based on the steady state temperature of an internal heating rate (Section 3.2) close to the present-day Chondritic Earth value. This is a rather low temperature as an initial condition, but it suffices the purpose of demonstrating the effects of exoplanetary mass and surface temperature on their thermal history. The choice of initial condition is improved in the dynamical models (Section 4.3.1) where a steady state temperature profile just below the corresponding solidus of the planet is used as the initial condition.

Symbol	Description	Value/Formular	Unit
r_m	Mantle radius	–	km
r_c	Core radius	–	km
g_0	Surface gravity	–	m s^{-2}
T_{surf}	Surface temperature	–	K
ΔT_{surf}	Temperature contrast across surface thermal boundary	$T_m - T_{surf}$	–
ΔT_{cmb}	Temperature contrast across CMB thermal boundary	$T_{cmb} - T_m$	–
c_{p-m}	Specific heat of the mantle	1250	$\text{J K}^{-1} \text{kg}^{-1}$
c_{p-c}	Specific heat of the core	550	$\text{J K}^{-1} \text{kg}^{-1}$
ρ_m	Average mantle density	–	kg m^{-3}
ρ_c	Average core density	–	kg m^{-3}
η	Uniform viscosity	2.5×10^{23}	Pas
$H(t)$	Internal heating rate per unit mass	$H(t) = H_0 \left(\frac{1}{2}\right)^{t/\tau}$	W kg^{-1}
H_0	Internal heating rate at time zero	–	W kg^{-1}
τ	Effective half life of the decay of internal heating rate (fuel mix)	2.4	Gyrs
k_m	Thermal conductivity of mantle material	4.7	$\text{W m}^{-1} \text{K}^{-1}$
Ra_c	Critical Rayleigh number	1×10^3	–
α	Thermal expansivity	–	K^{-1}
κ	Mantle thermal diffusivity	$k_m / (\rho_m c_{p-m})$	$\text{m}^2 \text{s}^{-1}$
β	Power law exponent in Equation 3	0.33 (Turcotte and Schubert, 2002)	–

Table 1: Explanation of parameters used in parameterised model equations and model set-up (Table 2).

3.2 Modelling the effect of exoplanet mass

Planets of one, two, four, and eight times the Earth’s mass are modelled to investigate thermal evolutions of planets of different sizes. Van den Berg et al. (2010) modelled pseudo-compressible densities in exoplanets by introducing a uniform compression factor $f > 1$, applying the same factor to both the mantle and the core. They further assumed that the planets have a similar core-mass ratio ($X_c = 0.315$) as the Earth. Here we take the model m4, a planet with $f = 1.5$ and $8 M_\oplus$, of van

den Berg et al. as a reference model. This model is reproduced as a4 in Table 2. A linear increase of the compression factor f with planetary mass is modelled, from which mantle and core density values are calculated. Radii of the mantle and the core are calculated based on constant core-mass ratio (see van den Berg et al. 2010 for derivations). Table 2 describes these model parameters. All models include time-dependent internal heating. The initial heating rate is taken as the estimated present-day value of the Earth ($2.55 \times 10^{-12} \text{ W kg}^{-1}$). This relatively low initial internal heating rate is expected to result in slower cooling and, when applied to a planet of the Earth’s mass, result in lower corresponding surface heat flow levels than the estimated present-day surface heat flow on the Earth. Initial core temperature is taken as 7500 K. The specific heat of the core c_{p-c} is calculated such that the total heat capacity of the core is 0.44 times that of the mantle (van den Berg et al., 2010).

Models	f	r_m	r_c	g_0	ρ_m	ρ_c	mass	H_0
a1	1	6371.0	3486.0	9.80	5511.4	12951.8	1 M_\oplus	2.55×10^{-12}
a2	1.071	7341.9	4015.9	14.79	5902.7	13871.4	2 M_\oplus	2.55×10^{-12}
a3	1.214	8871.8	4852.8	20.26	6690.8	15723.5	4 M_\oplus	2.55×10^{-12}
a4	1.500	10416.7	5697.8	29.39	8267.1	19427.7	8 M_\oplus	2.55×10^{-12}

Table 2: Models investigating effects of planetary mass.

Results of the modelling experiments are shown in Figure 1. The temperature graph shows the evolution of the volume average temperature of the mantle. The surface heat flow graph displays total heat flow out of the top of the mantle layer. In the legend M denotes the mass of the Earth. We can see from these results that exoplanetary thermal history is strongly influence by planetary mass. A clear trend can be observed in the shift of curves in both graphs. The temperature rises in the first 3 Gyrs due to high internal heating rates and high initial heat flow across the CMB (to be added in Figure 1). The higher total energy produced by internal heating in planets of higher mass results in the higher peak temperatures. Due to the higher average temperatures of larger planets and their larger surface areas, total surface heat flow is much higher for larger planets. Model a4 has almost twice the surface heat flow than a1. Despite higher heat dissipation on the surface, planets with higher mass cool at a smaller rate. With higher mass and radius, the low surface to volume ratio of the planet slows down the cooling. As predicted, the surface heat flow level of the planet with 1 M_\oplus is lower than the observed present-day surface heat flux ($\sim 44 \text{ TW}$; reference) of the Earth, due to the low initial internal heating rate, which is much lower than the heating rate of the Earth in its early history ($\sim 4.5 \text{ Gyrs}$ ago).

3.3 Exoplanet surface temperature

Model a4 in Section 3.2 is used as a reference model, from which the surface temperature is varied according to Table 3. The initial average temperature is kept unchanged. In this way by changing surface temperature we are modelling different temperature contrasts between the surface and the interior. As we can see from Figure 2, the effects of changing the surface temperature by 300 K is on the same order of magnitude to varying the planetary mass by factors of 2, 4, and 8. Lower surface temperature results in higher surface heat flow due to higher contrast at the surface thermal

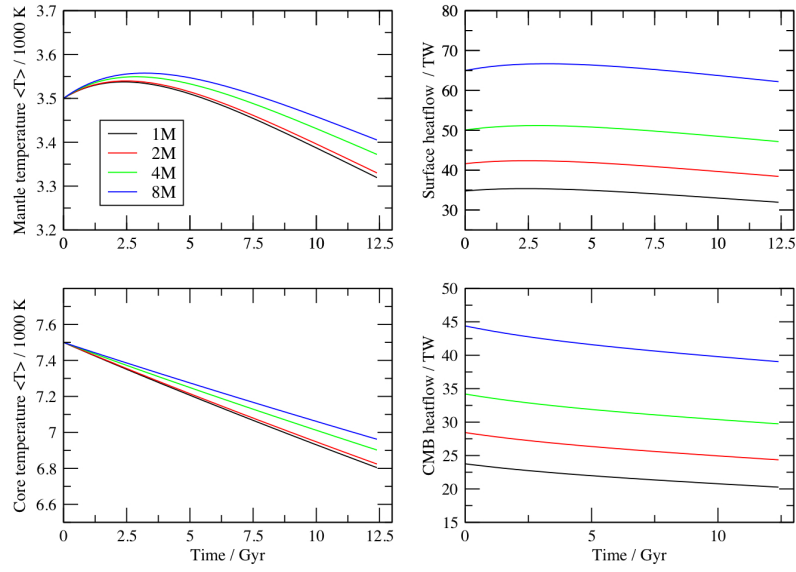


Figure 1: Thermal evolution of planets with different masses

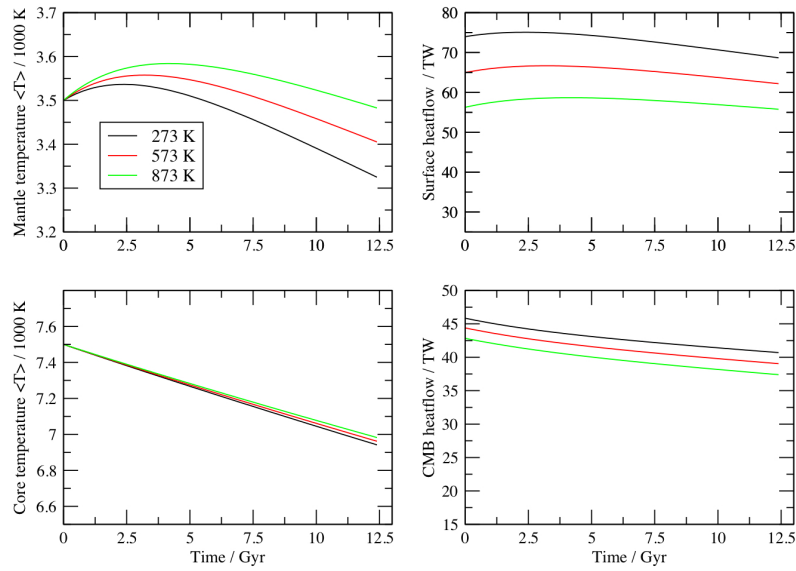


Figure 2: Thermal evolution of planets with different surface temperatures

Models	a4	b1	b2
T_{surf}	573	273	873
Amount of cooling in 12.4 Gyrs / K	94.9	175.2	17.4

Table 3: Parameterised convection models investigating effects of surface temperature, to be updated.

boundary layer. A planet with 300 K lower surface temperature results in around 80 K lower average temperature in 12.4 Gyrs time, which is about the same temperature difference between models a1 and a4 in Section 3.2. Such a difference is not negligible, especially in modelling long-term thermal histories. CoRoT-7b, a super-Earth discovered by the CoRoT mission in 2009 (NStED, 2011), has a close orbit to its star. Estimates of the planet’s surface temperature reach as high as 2500 K (Ziethe et al., 2011). Such a high surface temperature may slow down the cooling of the planet considerably. Strong heterogeneity in the surface temperature is also expected for CoRoT-7b due to tidal locking. These factors should be taken into consideration when modelling the planet’s thermal state and they may result in local partial melting and strong lateral variations in the thermal structure.

3.4 Comparison with dynamical models

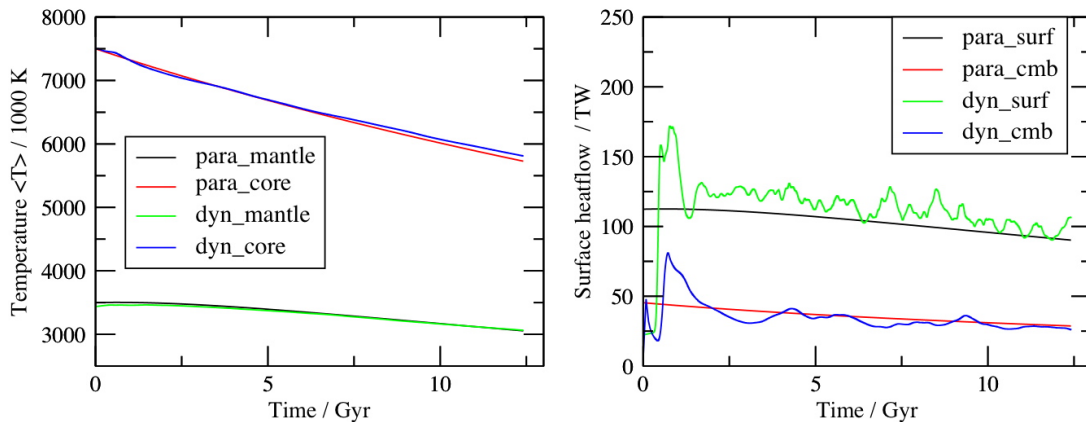


Figure 3: Comparison between parameterised convection models and dynamical models for planet with Earth-like core-mass ratio

Corresponding parameters are implemented in parameterised and dynamical models to compare these two different modelling approaches, and to test the potential uncertainties introduced by using the parameterised modelling approach as a simplification to the dynamical approach. a4 is taken from Section 3.2 and compared to the corresponding dynamical model. Core–mantle thermal coupling is considered in this model. The formulation and numerical methods of the corresponding dynamical models are described in Section 4.1. The initial internal heating rate is taken as $2.55 \times 10^{-12} \text{ W kg}^{-1}$ in both models.

Both mantle and core temperatures are plotted in the first frame of Figure 3. In the second frame, total heat flow values across the surface and CMB are plotted. The mantle and core temperatures obtained with these two modelling approaches agree with each other very well. Heat flow values of the dynamical model has strong fluctuations but are well-approximated by the heat flow values of the parameterised model. This shows that for models with uniform viscosity including the thermal coupling between the mantle and the core, as used in Sections 3.2 and 3.3, the parameterised modelling approach is a reasonable simplification to the dynamical approach.

4 Dynamical models

Here I present the modelling experiments with full convection, or dynamical models, that provide more details of the thermal state of evolving planets than the parameterised convection models. Two series of super-Earth models are used to investigate the effects of core-mass fraction. Both series are models of 8 times the Earth’s mass. In one series the planets have a core-mass fraction similar to that of the earth (referred to as ‘core models’ in the following text). In the other series, planets with a zero core size are investigated as an end member to see the role of the core size in the thermal evolution of the planet (referred to as ‘core-less models’). In the series of core models, a depth-dependent viscosity model is investigated in both evolutionary and equilibrium (steady state) models. In the series of core-less models, their steady state temperatures are first investigated with respect to viscosity and internal heating rate. Then the thermal evolutions of corresponding core and core-less models are compared. The thermal coupling between the core and the mantle is considered in the core models.

4.1 Governing equations

The governing equations for thermal convection in a highly viscous medium in the (extended) Boussinesq approximation are the following three equations derived from conservation principles. Solid state phase transitions (van den Berg et al., 2010) are not included in the present model.

1. Conservation of mass

$$\partial_j u_j = 0 \tag{6}$$

2. Conservation of momentum

$$-\partial_i \Delta P + \partial_j \tau_{ij} = Ra (\alpha T) g(r) \hat{e}_{ri} \tag{7}$$

$$\tau_{ij} = \eta(P) e_{ij} \tag{8}$$

3. Conservation of energy

$$\frac{DT}{Dt} = \partial_j (\kappa(r) \partial_j T) + \alpha g(r) Diw(T + T_0) + \frac{Di}{Ra} \Phi + R_H H(t) \tag{9}$$

4.2 Numerical techniques and resolution

The dynamical models apply finite element techniques using the SEPRAN package (Segal and Praagman, 2000). Equations are solved in a spherical axisymmetric domain where the extended Boussinesq approximation is applied (Schubert et al., 2001). Two different meshes are created

according to the core sizes of the two series of models. In the mesh for planets with a finite core heat reservoir, element boundaries include concentric curves and radiating lines from the planet’s centre. Such a mesh is not suitable for a core-less planet because elements would tend to be very narrow with an aspect ratio (width over height) much smaller than one toward the planet’s centre. Therefore we use a different set-up for core-less models such that there is still a regular mesh at its centre. For models with a core (left, Figure 4), the domain contains 20301 nodal points, 201 on Curve 3 and Curve 1, and 101 on each of Curve 2 and Curve 4. For core-less models (right, Figure 4), the unknown domain contains 39758 nodal points, 451 on Curve 2, and 151 on each of Curve 3 and Curve 1.

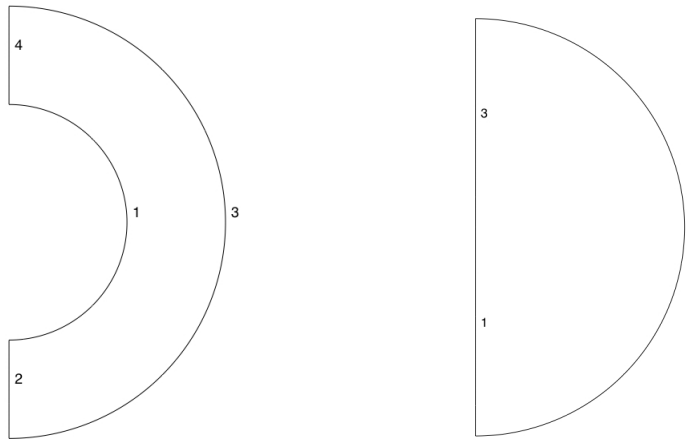


Figure 4: Meshes used in two series of dynamical models.

4.3 Exoplanets with an Earth-like core-mass fraction

4.3.1 Modelling the effects of depth-dependent viscosity

The temperature dependence of viscosity has been known for a long time and has been well emphasised by early researchers (Schubert et al., 1979; Christensen, 1985). Commonly in models of planetary thermal evolution or internal structure, viscosity is prescribed in a simple power-law relation with temperature (Davies, 1980; Valencia et al., 2006). It has been well established that viscosity is dependent not only on temperature but also pressure (Turcotte et al., 2002). Especially in large exoplanets where internal pressure close to the CMB can reach over 1 TPa (van den Berg et al., 2010), the depth dependence of viscosity may be more prominent. Therefore it is necessary to investigate the effects of the depth dependence of viscosity on exoplanetary thermal evolution.

I will compare models with uniform viscosity and a depth-dependent viscosity profile, where horizontal homogeneity is assumed. An Arrhenius type of viscosity formulation (Equation 11) is used in the calculation of a viscosity profile, which is then implemented as a time-independent piece-wise linear profile in corresponding dynamical models. The choice of parameters for the calculation of this viscosity profile is given in Appendix A. With the temperature and pressure dependence of the viscosity model unchanged, the viscosity prefactor is varied to search for a viscosity profile that yields the

same volumetric average as the uniform viscosity (2.5×10^{23} Pa·s). In this way we are modelling only the distribution of viscosity, and its effect on thermal evolution and steady state temperature. We use the same viscosity scale as parameterised models (Section 3.1). The resulting viscosity profile is presented in Figure 5, left. Viscosity increases with decreasing temperature and increasing pressure. In planetary interior, temperature increases while pressure decreases with depth. The viscosity is high at the surface because of its very low temperature. It then rapidly decreases with depth due to the increase of temperature in the surface thermal boundary layer. For the bulk of the mantle, viscosity increases despite rising temperature, because of its pressure dependence. At the bottom of the mantle, viscosity decreases again due to rapid increase of temperature at the CMB thermal boundary layer.

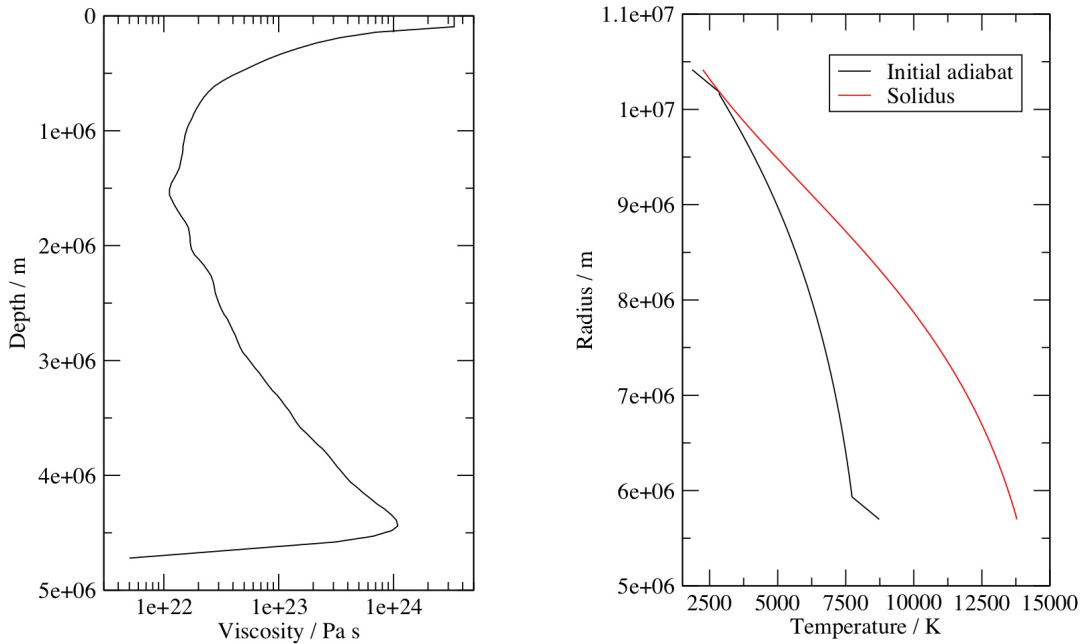


Figure 5: Depth-dependent viscosity profile and initial temperature profile of core planets

This viscosity profile is implemented in both steady state models and evolution models to test its effects on steady state temperature and thermal history.

4.3.2 Model description

Four modelling experiments are performed to investigate the effects of depth-dependent viscosity on exoplanet thermal evolution and steady state temperatures. The parameterisation of these models are tabulated in Table 4 and 5. Models A1 and A3 use a uniform viscosity equal to the viscosity scale value, while A2 and A4 use the depth-dependent viscosity profile (Section 4.3.1). Models A1 and A2 are thermal evolution models with decaying internal heating. They are compared to investigate the effect of the depth-dependent viscosity profile on thermal evolution. Models A3 and A4 are equilibrium models to test whether depth-dependent viscosity would change the steady state temperature of a certain internal heating rate.

These four models are based on the model labelled m4 in (van den Berg et al., 2010). According to this model, a compressibility scaling factor $f = 1.5$ is applied to uniform mantle and core densities. The corresponding planetary radius and core radius can be calculated based on a core-mass ratio of $X = 0.315$, similar to that of the Earth. The gravitational acceleration is computed along the radius based on uniform densities for the core and mantle, consistent with the dynamical model formulation. A uniform gravity distribution is assumed for the mantle due to the large gravitational effects of the core. According to van den Berg et al. (2010), thermal expansivity may decrease with depth by a factor of 20 in the interior of super-Earths, due to high internal pressure. This has strong influence on the calculation of the initial adiabatic temperature profile. A decreasing expansivity is applied based on $\alpha(z) = \frac{\Delta\alpha}{[c(1-z)+1]^3}$, where the bottom/top expansivity contrast $\Delta\alpha = 0.05$ and $c = \Delta\alpha^{1/3} - 1$.

The initial condition is chosen such that the subsolidus convection starts at an adiabatic temperature profile (including thermal boundary layers) just below the solidus (Figure 5, right). The solidus and adiabatic profiles are calculated accordingly to a compressible density profile, which is computed iteratively such that it would have a global average the same as the uniform density used in m4 of (van den Berg et al., 2010). The solidus profile is calculated according to the mantle solidus extrapolation of (Zerr et al., 1998), based on the Lindermann melting law (Zerr and Boehler, 1994) and a power-law relation between the Grüneisen parameter and density (Boehler and Ramakrishnan, 1980). The calculation of these profiles can be consulted in Appendix B. Based on the discussion in Section 2.1.2, the initial internal heating rate is computed such that its corresponding steady state temperature is equal to the global average of the initial adiabat. A localised perturbation is used on top of the initial temperature profile to initiate convection. The non-dimensional amplitude of the perturbation temperature is 0.1. It is located close to Curve 4 (left, Figure 4), at half the depth of the mantle layer. The initial thickness of surface and CMB thermal boundary layers is prescribed as 236 km. This thickness is calculated based on the parameterised convection approach, in which the surface boundary layer thickness $d = D(Ra/Ra_c)^{-\beta}$ (See Section 3.1 for the meaning of the symbols). The CMB boundary layer thickness is taken the same as the surface thermal boundary, based on observations made in previous dynamical models. These prescriptions of boundary layer thicknesses turn out to be good estimations. A constant surface temperature of 573 K is prescribed. Thermal coupling between the core and the mantle is considered in all dynamical models, in which a time-dependent essential boundary condition is used at the CMB, as the core temperature is updated at each time step. Other boundary conditions include free slip impermeable conditions on all boundaries, and zero horizontal temperature gradient along the axis of symmetry.

Models	A1	A2	A3	A4
Viscosity model	$\eta = \eta_0$	$\eta = \eta(P)$	$\eta = \eta_0$	$\eta = \eta(P)$
Internal heating model	$H = H(t)$	$H = H(t)$	$H = H_0$	$H = H_0$
Core coupling	on	on	on	on
Rayleigh number	2.244×10^8	2.244×10^8	2.244×10^8	2.244×10^8

Table 4: Dynamical models of planets with an Earth-like core-mass fraction

Symbol	Description	Value/Formular	Unit
η_0	Viscosity scale value	2.5×10^{23}	Pa s
H_0	Initial internal heating rate	6.6×10^{-12}	W kg ⁻¹
τ	Effective half life of the decay of internal heating rate (fuel mix)	2.4	Gyrs
r_m	Mantle radius	1.0417×10^7	m
r_c	Core radius	5.698×10^6	m
g_0	Surface gravity	29.38	m s ⁻²
T_{surf}	Surface temperature	573	K
c_{p-m}	Specific heat of the mantle	1250	J K ⁻¹ kg ⁻¹
c_{p-c}	Specific heat of the core	550	J K ⁻¹ kg ⁻¹
ρ_m	Uniform mantle density	8267.1	kg m ⁻³
ρ_c	Uniform core density	19427.7	kg m ⁻³
η_0	Viscosity scale value	2.5×10^{23}	Pa s
-	Initial core temperature	7500	K

Table 5: Parameters used in dynamical models

4.3.3 Results

The time series of the volumetric average temperature and surface heat flux of A1 and A2 are presented in Figure 6. As we can see from the figure, the mantle temperature of A2 decreases slower whereas its core temperature evolves at approximated the same rate as that of A1. This indicates slower cooling of the mantle but unchanged thermal coupling between the mantle and the core with depth-dependent viscosity. The surface heat flow of A1 slowly decreases from ~ 250 TW to ~ 150 TW in 12 billion years after the onset of convection. The surface heat flow of A2, however, remains more or less at the average level of 100 TW. Less fluctuation is observed in A2 surface heat flow. The general low surface heat flow in A2 explains the slower cooling of the mantle. Its relatively stable evolution suggest that thermal instabilities close to the surface are less vibrant.

Despite the higher mantle temperature of A2 and its low surface heat flow level, the heat exchange at its CMB is almost the same as in A1. The reasons for this can be investigated by inspecting the vertical profiles in Figure 7. The left two frames of Figure 7 present the temperature and velocity amplitude profiles at 10.243 Gyr, a snapshot chosen to represent internal conditions when convection has been well developed. As we can see in these two frames, A2 has a thicker surface thermal boundary layer. The lower surface geothermal gradient explains the lower heat flow values. At the bottom thermal boundary layer, temperature contrast is lower for A2 and the layer thickness is smaller. The similar thermal gradients at this boundary layer explain the similar CMB heat flow of A1 and A2. In the lower mantle, the temperature of A2 is lower than A1, which may be explained by the higher velocity of A2 in this region. The relatively low viscosity (Figure 5, left) in the lower third of the mantle of A2 mobilises this region, which result in higher convective velocity and faster heat transport. The average mantle temperature of A2 may be accounted for by its slightly higher temperature in the upper mantle, which strongly influence the global average temperature due to the spherical geometry of the planet. Though velocity is relatively high in the surface 1500 km of A2, its temperature in this region is not lower. The high convective motions in this region do not result in higher surface heat flow due to the lower geothermal gradient in the surface boundary layer. The two right-hand-side frames of Figure 7 are overlaying plots of all velocity profile snapshots of

A1 and A2. There are 80 snapshots in total for each model. This figure is produced to see if there is any pattern in the velocity profiles and to test whether existing patterns in A2 correlate with the viscosity profile. There is in general a low velocity zone at depths 1000-2500 km. This corresponds to a low-viscosity region in the depth-dependent viscosity profile.

Four temperature snapshots of each model are presented in Figure 8. The first three snapshots illustrate the onset of convection, while the fourth snapshot shows the mantle thermal state when convection has been well developed. The fourth snapshot corresponds to the profile snapshots in the left two frames of Figure 7. As we can see in the 2-D temperature profiles, convection starts from thermal instabilities close to the surface in A1. In A2, however, convection starts mainly with thermal instabilities close to the CMB, while no downwelling is observed close to the surface. At 10.243 Gyr, convection in A1 is marked by both downwelling flows from the surface and upwellings from the CMB. Convective patterns in A2 are different, marked by wide thermal instabilities at the CMB and only minor visible downwelling from the surface.

Some of the above observations can be explained by the depth dependence of viscosity. The relatively low viscosity at the bottom of the mantle serves to mobilise this region and lowers the lower mantle temperature in A2. The high viscosity of A2 suppresses convective instability and results in relatively stable conduction at the surface.

Equilibrium model results are presented in Figure 9. Both mantle and core steady state temperatures are higher in A4. This means that planets with such a depth dependence of viscosity starts subsolidus cooling with a lower internal heating rate. Depth-dependent viscosity results in delayed cooling.

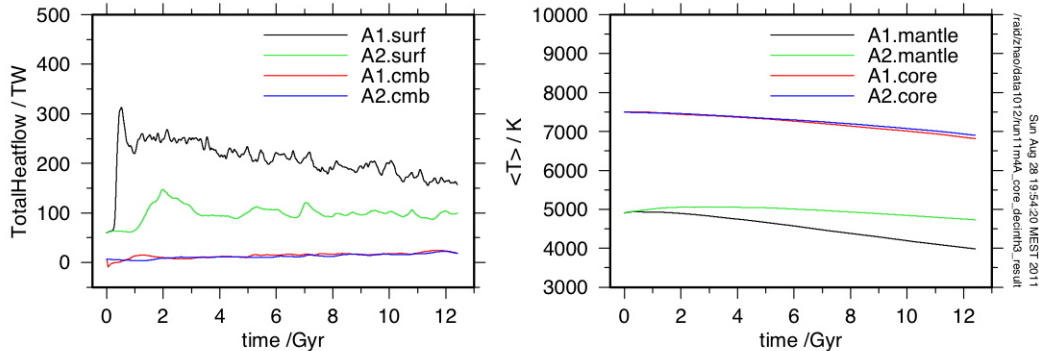


Figure 6: Time series of temperature and heat flow values of A1 and A2

4.4 Core-less exoplanets

4.4.1 The internal conditions of core-less planets

With a planet’s total mass unchanged, the smaller the core of the planet, the bigger the planet would be, because the core has a much higher density than mantle material. The size of the core also has a strong influence on the gravity field in the interior of the planet. Since the core consists

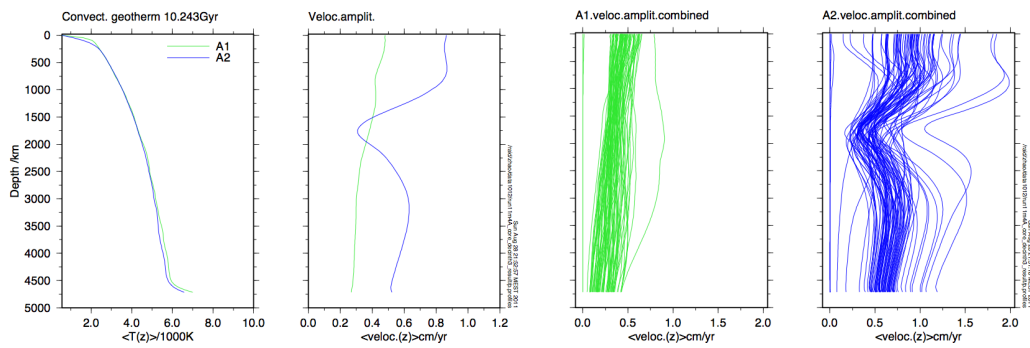


Figure 7: Temperature and velocity profiles of A1 and A2

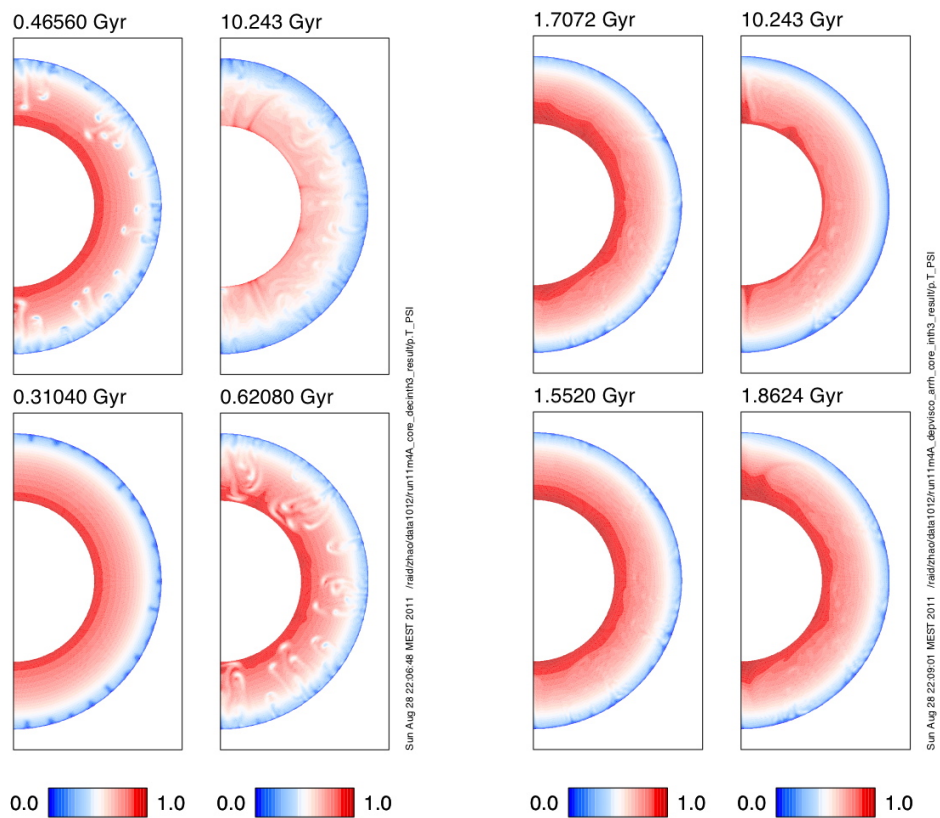


Figure 8: 2-D temperature plots of A1 and A2

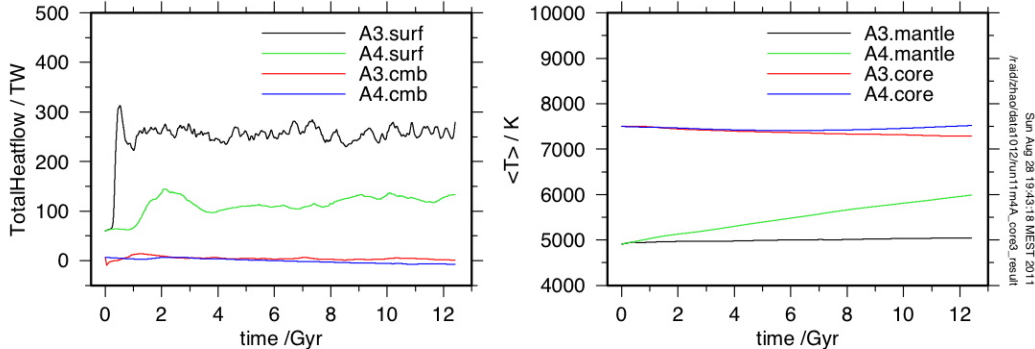


Figure 9: Time series of temperature and heat flow values of A3 and A4

of very dense material, the bigger the core, the higher gravitational acceleration at the CMB, and the smaller the relative gravity variation through the mantle. The combined effects of planetary size and internal gravitational variations result in very different internal conditions inside planets with different core sizes. In our study, we model the mass ratio of the core to the mass of the whole planet, and study how the internal temperature, pressure, and gravitational conditions change accordingly. The effects of these changes on subsolidus cooling history of the planet is investigated in subsequent steady state and evolutionary modelling experiments in Sections 4.4.2 and 4.4.3.

A planet with a zero metal core size and $8 M_{\oplus}$ is studied as an end member. The density profile of this planet is approximated according to a pressure-dependent compressibility model similar to the Murnaghan first-order equation of state, until convergence is achieved. Material properties are taken from post-perovskite, which is assumed to be a representative material for large exoplanets. The solidus is calculated in a similar way as in Section 4.3.2. Details of the calculations can be found in Appendix B. Such a planet has a radius of 1.3459×10^4 km and a global average density of 4.679×10^3 kg/m³. The pressure at its CMB is 689.4 GPa. The adiabatic temperature profile just below the solidus is computed to be used as the initial condition of thermal evolution models. Such an adiabat has a surface potential temperature of 1935 K, and reach 6177.6 K at the CMB. Core-less planets therefore have very different internal conditions than planets with an Earth-like core-mass ratio. If subsolidus thermal convection occurs on such a planet, the convective regime is a sphere without a bottom boundary surface. Convective cells, if they exist, may not reach the centre of the planet. Thus the convective behaviours may be very different than those observed in models with an Earth-like core-mass ratio. These convective behaviours are explored in the series of steady state and evolutionary models in the following sections.

4.4.2 Modelling the steady state temperature in core-less planets

In this section I investigate the steady state temperatures of core-less models and compare them to the corresponding solidus. The steady state temperatures are firstly studied in preliminary calculations based on parameterised models. When the heating rate and global average temperature are constant, the steady state temperature can be calculated analytically using the parameterised relation (See Section 3.1 for equations). This relation between steady state temperature, internal

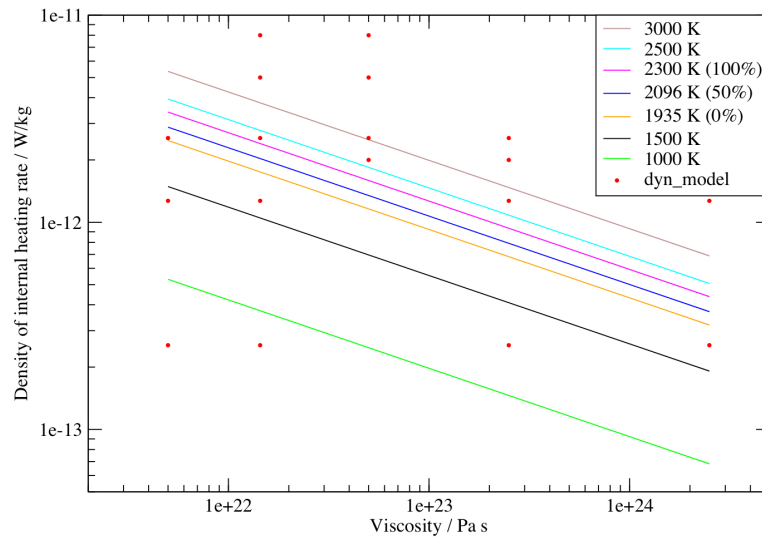


Figure 10: Steady state temperatures of core-less planets

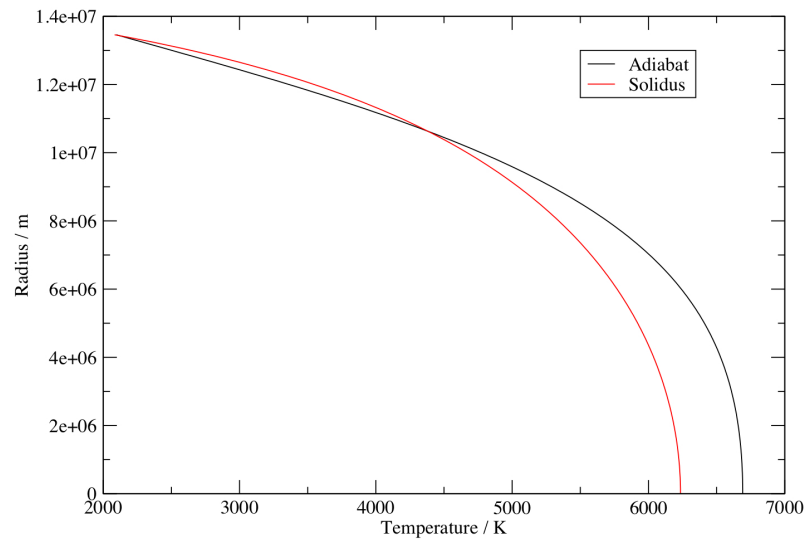


Figure 11: The solidus of core-less planets and the adiabatic temperature profile that corresponds to 50% melting

heating, and viscosity can be expressed as in Equation 10, where H is the constant internal heating rate, η the uniform viscosity, and $\Delta T = T_{avg} - T_{surf}$ (see Section 3.1 for meanings of the other symbols).

$$H = \frac{S_{surf}k}{\rho_m D} \left(\frac{\rho g \alpha D^3}{Ra_c \kappa} \right)^\beta \frac{\Delta T^{\beta+1}}{\eta^\beta} \quad (10)$$

Using this relation, steady state temperatures are calculated with respect to variable internal heating and viscosity values. Results are plotted in Figure 10 as isolines of steady state temperature. The steady state temperature increases with increasing internal heating rate or viscosity. Note that logarithmic scales are used in both axes of Figure 10. These steady state temperatures are volumetric averages, and they are expanded as adiabatic temperature profiles for core-less planets which has the global average as the steady state temperature. These adiabatic temperature profiles are then compared with the solidus (Section 4.4.1). A melting percentage is calculated by integrating the volume of melt along the radius assuming horizontal homogeneity. Key percentages are marked in Figure 10. In Figure 11, the adiabat that results in 50% melting (corresponding to a potential temperature of 2096 K and global average of 4349 K) is illustrated with the solidus. As we can see from this figure, different than planets with an Earth-like core-mass ratio where melting starts in the upper mantle, core-less planets start melting in the lower half of their mantle, when the adiabat is increase above the solidus.

The steady state temperatures presented in Figure 10 are much larger than those expected for planets with an Earth-like core-mass ratio. For example, a core planet with a viscosity of 2.5×10^{23} Pa.s and internal heating rate of 2.55×10^{-12} W kg $^{-1}$ has a steady state temperature of 3500 K, while that of the core-less planet is above 4000 K. High steady state temperatures can be explained by slower cooling expected on core-less planets due to their large size and large internal heat production. Core-less planets may be a thermal regime of periodic melting. The slow cooling rates result in heating and (partial) melting of the planet. The melting may in turn facilitate efficient cooling and result in rapid decrease of temperature to below the solidus. The planet may then solidify and be heated again, and go through cycles of heating, melting, rapid cooling, and solidifying. It has been suggested that Venus has gone through such periodic melting.

Dynamical equilibrium models are then performed to further investigate steady state temperatures of core-less planets. Internal heating–viscosity combinations that have been investigated by dynamical models are denoted as red dots in Figure 10. The results of these dynamical models suggest a similar trend but tend to give higher steady state temperatures. This may be due to the implicit assumptions made in the parameterisation of surface heat flow in the parameterised approach. While in parameterised calculations, the total radius of the core-less planets is used as the depth of the convecting layer, this would hardly happen in the dynamical model due to the geometry close to the centre of the planet. The discrepancy between steady state temperatures calculated by parameterised equations and by dynamical modelling experiments is likely due to the unrealistic parameterisation of the former. The convective behaviours of core-less planets are further explored in the following section.

4.4.3 Thermal evolution of core-less planets

The thermal histories of planets with an Earth-like core-mass fraction and core-less planets are

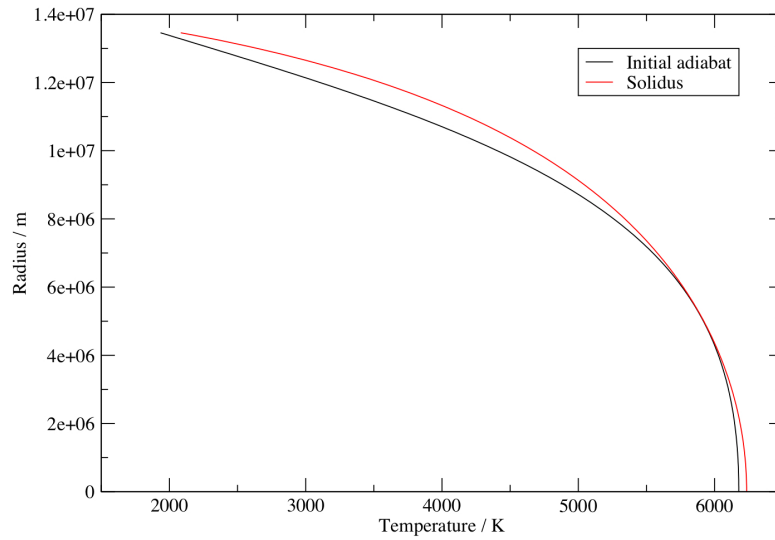


Figure 12: Initial temperature profile of core-less planets

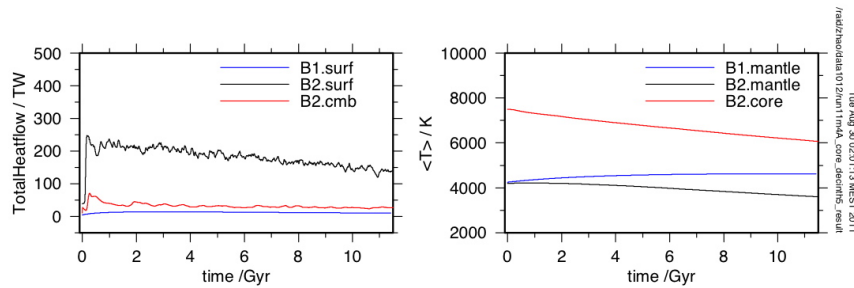


Figure 13: Time series of temperature and heat flow in B1 and B2

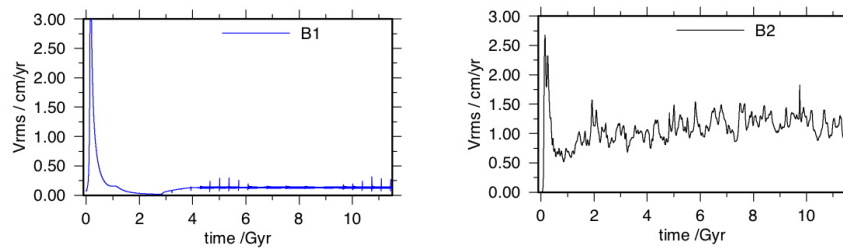


Figure 14: Times series of the average velocity amplitude in B1 and B2

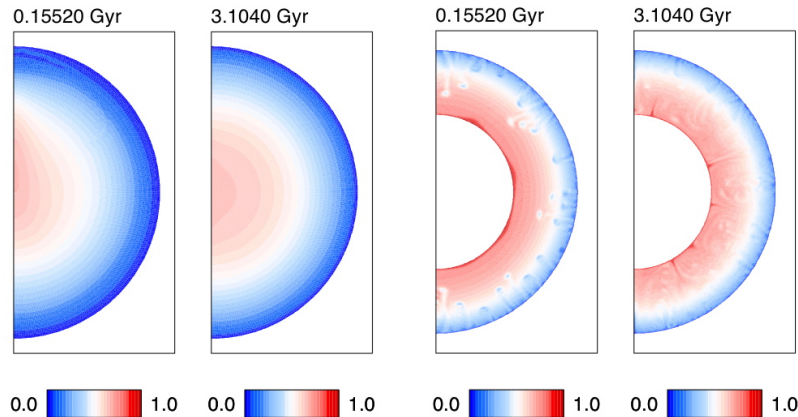


Figure 15: 2-D temperature plots of B1 and B2

compared in this section. Uniform viscosities are taken as prescribed as the viscosity scale value (Table 5). The initial temperature profile is computed such that it is just below the solidus of corresponding core-less planets, which is a lower threshold than the solidus of core planets. The adiabatic extrapolation of the initial average temperature is presented in Figure 12. An initial internal heating is then calculated so that its steady state temperature is the global average of the chosen initial temperature profile. The initial internal heating thus obtained is $5.32 \times 10^{-12} \text{ W kg}^{-1}$. B1 is the core-less model and B2 is the corresponding model of an Earth-like core-mass fraction. Model parameters are listed in Table 6.

Results of B1 and B2 are presented in Figures 13 to 15. We can see from these figures that the core-less planet cools slower. With the same initial average temperature, the core-less planet has a temperature $\sim 1000 \text{ K}$ higher than the core planet, after 11.5 Gyrs. Surface heat flow is very low, and evolves in a very stable manner. From the comparison of 2-D temperature plots, we can see that, apart from the onset of convection, the core-less planet retains a well-stratified thermal structure. The average velocity of the core-less planet appears to have periodic peaks, but in general stay close to zero. We may infer from these results that thermal convection is not the main means of heat transport in a planet like B1, despite its relatively low uniform viscosity. Such inferences also explain the discrepancy between steady state temperatures calculated by the parameterised approach and those by the dynamical approach. The parameterised approach assumes that thermal convection occurs in the entire the mantle region except for relatively thin thermal boundary layers. Heat flow values calculated from such an assumption are high and would result in relatively low steady state temperatures.

4.4.4 Super-plumes

One of the interesting observations made in coreless planets is the initial ‘super-plume’, a strong flow of hot material from central areas to the surface at the onset of convection. This plume efficiently transports hot materials to the surface and thereby decrease the planet’s internal thermal gradient. Figures 16 and 17 illustrate such phenomenon. This model has very short output steps so that resolution is gained into the details of the relatively fast event. Input parameters are taken the same as model B2.

Models	B1	B2
η_0	5×10^{22}	5×10^{22}
H_0	5.32×10^{-12}	5.32×10^{-12}
Core coupling	-	on
Ra	4.997×10^9	1.122×10^9
$g(0)$	17.60	29.38
r_{mantle}	1.3459×10^7	1.0417×10^7
r_{core}	0	5.698×10^6
T_{surf}	3000	5000
ΔT (temperature scale)	5000	6250
Initial core temperature	-	7500
ρ_m	4679.0	8267.1
ρ_c	-	19426
cP_m	1250	1250
cP_c	-	550

Table 6: Model set-up of B1 and B2

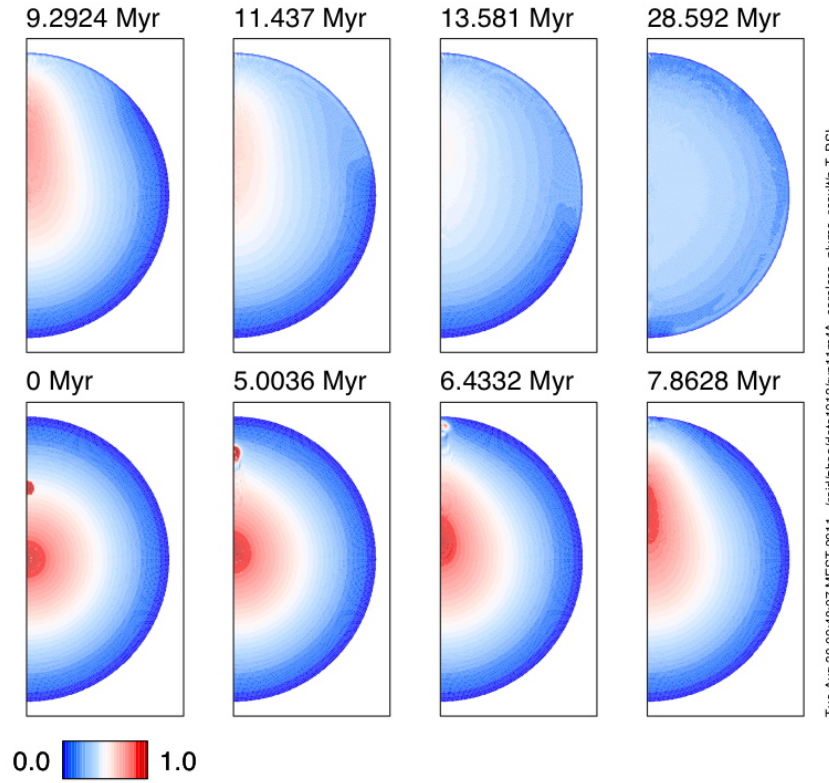


Figure 16: 2-D temperature plots of a super-plume in core-less planets

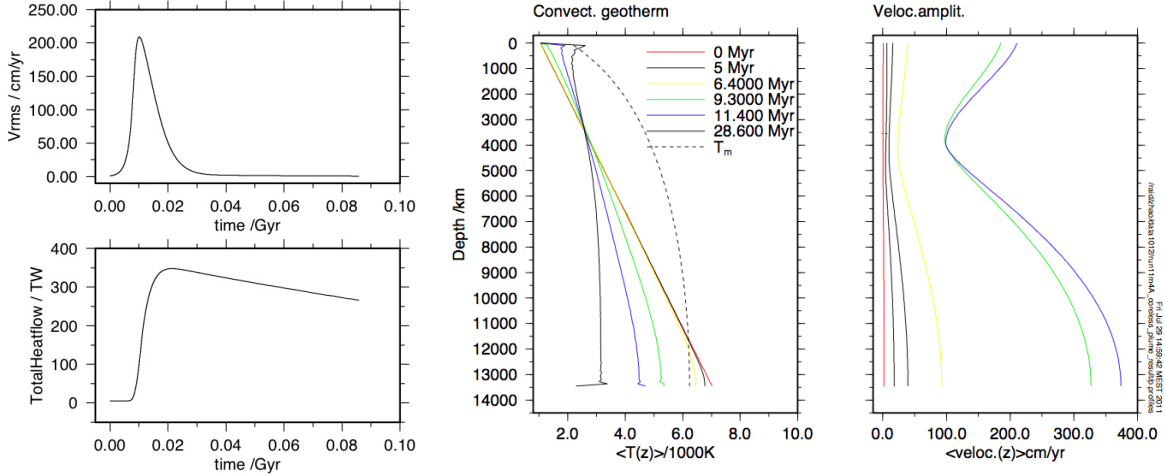


Figure 17: Time series of heat flow and velocity and temperature and velocity profiles during a super-plume event

5 Discussions and conclusion

In summary, larger planets in general cool slower from an initial hot state, due to larger total internal production of heat and relatively low surface-to-volume ratio. They also have ‘readjustment times’ much larger than the age of the universe (~ 13.7 Gyr), thus initial thermal conditions of these planets influence their thermal states throughout their history. It is therefore important to use reasonable specification of initial conditions, when modelling exoplanetary thermal history. Steady state temperatures obtained from equilibrium modelling experiments have been used as initial conditions, together with the corresponding internal heating level as the initial internal heating rate. With such specifications, it is made sure that the planet would cool from the initial condition, instead of heating up. This is a useful way of finding an initial condition for subsolidus cooling. If we use an initial condition just below the solidus of the planet, it is ensured that the planet cools in the subsolidus regime and that the thermal history modelled is a subsolidus history. If the initial temperature is higher, or the initial internal heating rate is higher, the planet is expected to be (partially) molten.

However, the approach of using a steady state temperature just below the solidus as an initial condition is not necessarily the only initial condition from which a planet may start subsolidus cooling. An initially (at least partially) molten planet may experience accelerated cooling such that at certain moments it reaches a temperature lower than the steady state temperature of its internal heating. If the planet solidifies at such a moment and cooling slows down to the level governed by subsolidus cooling relations, it is expected to heat up again. If this heating (partially) melts the planet again, this planet may enter a periodic melting regime until internal heating decays to such levels that no more melting would occur. It is also possible that the planet which solidifies has an internal heating level whose corresponding steady state temperature is lower than the solidus. This is well possible because of the large ‘readjustment time’ of large exoplanets. A large amount of the primordial heat may still remain in the planet while internal heating decays faster than the loss of the primordial heat. If the subsolidus cooling of a planet starts at an internal heating level

whose steady state temperature is lower than the solidus, this planet is expected to cool faster due to relatively low heat production. By using a temperature profile just below the solidus and the internal heating rate whose steady state temperature corresponds to such a temperature profile, we are modelling the slowest-cooling end member of all possible subsolidus cooling histories of an exoplanet. Without more information, there are large uncertainties involved in the choice of the initial condition for the study of exoplanetary thermal history. But the approach mentioned above ensures that the thermal evolution starts just after solidification and stays in the subsolidus regime, and it suffices the purpose of systematic modelling investigations of parameter variations.

A depth-dependent viscosity distribution calculated from an Arrhenius type of formulation are found to result in a lower cooling rate than a corresponding uniform viscosity model. In thermal equilibrium models, such viscosity distribution results in higher steady state temperatures for both the core and especially the mantle. This means that a planet with strong depth dependence of its viscosity distribution is likely to enter subsolidus cooling later. Depth-dependent viscosity suppresses surface thermal instabilities and mobilise the low-viscosity zones in the upper part and the bottom of the mantle layer, and thereby influences the thermal structure of the planet. When the depth-dependence of viscosity is considered, convective motion is propelled by warm upwellings close to the core mantle boundary while the surface is characterised by a thick boundary layer of stable conduction.

Viscosity is always dependent on pressure in planetary interiors. But at higher pressures, there is more uncertainty associated with this dependence. It is commonly believed that viscosity increases with depth, which would result in decreased convective vigour at greater depth in large terrestrial planets. Recent findings suggest that viscosity in the interior of large terrestrial exoplanets may be lower than expected for two reasons. Firstly, the mantle of a super-Earth mostly consists of post-perovskite (PPv), which, based on new calculations (Ammann et al., 2010), has lower viscosity than perovskite by two to three orders of magnitude. Secondly, mineral physics studies suggest that viscosity may possibly decrease when pressure exceeds ~ 0.1 TPa (Karato, 2010). If viscosity is indeed lower at depth in large terrestrial exoplanets, it is expected to mobilise the lower mantle and increase the thermal coupling between the core and the mantle. In this way the mantle may cool slower while the core cools faster. It is therefore important that future models of the thermal history of large exoplanets consider the effects of depth dependence of viscosity, especially when making inferences of the cooling rate and thermal structure.

In my studies the depth-dependent viscosity is parameterised such that the temperature and pressure dependence is only considered in a spatial sense, not in a temporal sense. When time dependence is considered, the early viscosity of a cooling planet would be lower and increases as the planet cools. This would result in faster cooling at the beginning and slower cooling later on. But the depth-dependent viscosity models in this study are a reasonable first attempt to study the effects of a non-uniform viscosity distribution along the radius, as opposed to uniform viscosity formulations.

The core size of a planet has a strong influence on its internal conditions, through its influence on planetary size and the gravitational acceleration distribution. In their early history, planets with a smaller core are more likely to be in a thermal regime of periodic melting than those of an equal mass and larger core, their subsolidus cooling being accordingly delayed. This is due to very high steady state temperatures and relatively low melting temperatures. Such is a combined effect of

larger planetary size, rapid decrease of gravitational acceleration with depth, and lower compressibility of density. It is also questionable whether thermal convection would be the main means of heat transport inside a core-less planet. Subsolidus cooling of these planets starts at a relatively low temperature, due to their high possibility of periodic melting. As suggested by model results, this cooling history may be dominated by steady heat conduction combined with quasi-periodic thermal instabilities. Moreover, “Super-plumes” are observed in planets without a metal core, which efficiently transport hot materials to the surface and thereby decrease the planet’s internal thermal gradient. With the CoRoT and Kepler space missions, more terrestrial exoplanets will be detected using the transit method. The volume of these planets inferred from transit measurements can be combined with information of their total mass obtained by subsequent radial velocity observations. The average density thus estimated can be used to infer the possible core mass fraction of the planet. This information must be considered in modelling the thermal history of these planets.

6 Acknowledgement

I would like to express my gratitude firstly to my supervisor Dr. Arie van den Berg, for his guidance, encouragement, and stimulating discussions for a whole year. I would also like to thank my family and friends for their generous support. Special thanks goes to Ole, whose love and support has made the writing of the thesis possible.

References

- Ammann, M. W., J. P. Brodholt, J. Wookey, D. P. Dobson. 2010. First-principles constraints on diffusion in lower-mantle minerals and a weak D layer. *Nature* 465, p.462-465.
- van den Berg, A. P., E. S. G. Rainey, D. A. Yuen. 2005. The combined influences of variable thermal conductivity, temperature- and pressure-dependent viscosity and core–mantle coupling on thermal evolution. *Phys. Earth Planet. Inter.* 149, p.259-278
- van den Berg, A. P., D. A. Yuen, G. L. Beebe, and M. D. Christiansen. 2010. The dynamical impact of electronic thermal conductivity on deep mantle convection of exosolar planets. *Phys. Earth Planet. Inter.* 178, p.136-154
- Boehler, R., and J. Ramakrishnan. 1980. Experimental results on the pressure dependence of the Grüneisen parameter: a review *J. Geophys. Res.* 85(B12), p.6996-7002
- Boehler, R. 2000. High–pressure experiments and the phase diagram of lower mantle and core materials. *Review of Geophysics.* 38, p.221-245
- Borucki, W. J., *et al.* (65 additional authors not shown). 2011. Characteristics of planetary candidates observed by Kepler, II: Analysis of the first four months of data. *Astrophysics*, submitted. Latest manuscript accessible: <http://xxx.lanl.gov/abs/1102.0541v1>.
- Christensen, U. R. 1985. Thermal evolution models of the Earth. *J. Geophys. Res.* 90, B4, p.2995-3007
- Davies, G. F. 1980. Thermal histories of convective Earth models and constraints on radiogenic heat production in the Earth. *J. Geophys. Res.* 85, B5, p.2517-2530

- Fortney, J. J., M. S. Marley, J. W. Barnes. 2007. Planetary radii across five orders of magnitude in the mass and stellar insolation: application to transits. *The Astrophysical Journal*. 659, p.1661-1672
- Giannandrea, E., and U. Christensen. 1993. Variable viscosity convection experiments with a stress-free upper boundary and implications for the heat transport in the Earth's mantle. *Phys. Earth Planet. Inter.* 78, p.139-152
- Holland, K. G., and T. J. Ahrens. 1997. Melting of $(\text{Mg,Fe})_2\text{SiO}_4$ at the core-mantle boundary of the Earth. *Science*. 275, p.1623-1625
- Jet Propulsion Laboratory (JPL). 2011. California Institute of Technology. Accessed online on August 09, 2011. Accessible: <http://planetquest.jpl.nasa.gov/>
- Karato, S.. 2010. Rheological structure of the mantle of a super-Earth: Some insights from mineral physics. *Icarus*. Vol. 212, p.14-23
- McNamara, A. K., and P. E. van Keken. 2000. Cooling of the Earth: A parameterised convection study of whole versus layered models. *Geochem. Geophys. Geosyst.* 1, p.1027
- NASA/IPAC/NExSci Star and Exoplanet Database (NStED). 2011. Jet Propulsion Laboratory, California Institute of Technology. Accessed online on May 12, 2011. Accessible: http://nsted.ipac.caltech.edu/cgi-bin/bgServices/nph-bgExec?bgApp=/Sieve/nph-sieve&mission=NStED&uniqueid&viewfile=list_Planet_uniqueid&fromplanet
- O'Connell, R. J., and B. Hager. 1980. On the thermal state of the Earth. in: *Physics of the Earth's Interior*. ed. A. M. Dziewonski and E. Boschi. North-Holland. p.270-317
- O'Neill, C., and A. Lenardic. 2007. Geological consequences of super-sized Earths. *Geophys. Res. Lett.*, 34, L19204. (doi:10.1029/2007GL030598)
- Poirier, J. 1991. Introduction to the physics of the Earth's interior. *Cambridge University Press*.
- Seager, S., M. Kuchner, C. A. Hier-Majumder, B. Militzer. 2007. Mass-radius relationships for solid exoplanets. *The Astrophysical Journal*. 669, p.1279-1297
- Segal, A. and N. P. Praagman. 2000. The SEPRAN package. Technical report. Accessible: <http://ta.twi.tudelft.nl/sepran/sepran.html>.
- Schubert, G., P. Cassen, R. E. Young. 1979. Subsolidus convective cooling histories of terrestrial planets. *Icarus*. 38, p.192-211
- Schubert, G., D. L. Turcotte, P. Olson. 2001. Mantle convection in the Earth and planets. *Cambridge University Press*.
- Shirley et al Encyclopedia of planetary sciences. p809
- Sotin, C., O. Grasset, A. Mocquet. 2007. Mass-radius curve for extrasolar Earth-like planets and ocean planets. *Icarus*. 191, p.337-351
- Spohn, T., and G. Schubert. 1982. Modes of mantle convection and the removal of heat from the Earth's interior. *J. Geophys. Res.* 87, p.4682-4696

- Steinberger, B., A. R. Calderwood. 2006. Models of large-scale viscous flow in the Earth's mantle with constraints from mineral physics and surface observations. *Geophys. J. Int.* 167, p.1461-1481
- Tackley, P., H. van Heck, M. Ammann, J. Brodholt, D. Dobson. 2011. Mantle dynamics and plate tectonics on super-Earths: Effect of rheology. *Geophysical Research Abstracts*. Vol. 13, EGU2011-8567. EGU General Assembly 2011
- van Thienen, P., N. J. Vlaar, A. P. van den Berg. 2004. Plate tectonics on the terrestrial planets. *Phys. Earth Planet. Inter.* 142, p.61-74
- Turcotte, D., and G. Schubert. 2002. *Geodynamics*. 2nd ed. Cambridge Univ. Press.
- Valencia, D., R. J. O'Connell, and D. Sasselov. 2006. Internal Structure of massive terrestrial planets. *Icarus*. 181, p.545-554
- Valencia, D., R. J. O'Connell, and D. D. Sasselov. 2007. Inevitability of Plate Tectonics on Super-Earths. *Astrophysical Journal*. 670, L45. doi: 10.1086/524012
- Valencia, D., M. Ikoma, T. Guillot, and N. Nettelmann. 2010. Composition and fate of short-period super-Earths: The case of CoRoT-7b. *Astronomy and Astrophysics* 516, A20. (doi:10.1051/0004-6361/200912839)
- Wolszczan, A., and D. A. Frail. 1992. A planetary system around the millisecond pulsar PSR1257+12. *Nature* 355, 6356. p.145147. doi:10.1038/355145a0
- Zerr, A., and R. Boehler. 1994. Constraints on the melting temperature of the lower mantle from high-pressure experiments on MgO and magnesiowstite. *Nature*. 371, p.506-508
- Zerr, A., A. Diegeler, R. Boehler. 1998. Solidus of Earth's deep mantle. *Science*. 281, p.243-246
- Ziethe, R., P. Wurz, and H. Lammer. 2011. The Interior and Surface Environment of CoRoT-7b. *Geophysical Research Abstracts*. Vol. 13, EGU2011-14067. EGU General Assembly 2011

Appendix

A Depth-dependent viscosity

A program written in Fortran 90 is developed to calculate depth-dependent viscosity profiles for a given temperature profile. Temperature- and pressure-dependent formulations such as the Arrhenius model for Newtonian diffusion creep viscosity require substantial computational power and time. It is therefore beneficial to have a table of constant vertical viscosity values ready to be used in simpler model experiments. This allows for certain spacial viscosity resolution but reduces computational time significantly.

The temperature profile is read from the result of model A1 (Section 4.3.2) after it has achieved steady state. Corresponding pressure values are calculated assuming constant gravity, consistent with the formulation of dynamical models (Section 4.3.2). Viscosity profiles are calculated based on different viscosity models to test their suitability for dynamical models and to tune their parameters.

Both an Arrhenius type of viscosity and an exponential parameterisation are implemented in the program. The exponential model is a simplified form of the Arrhenius relations, and is commonly referred to as the Frank-Kamenetskii approximation. Parameters used in these models are explained and listed in Table 7. Results of some calculations are presented in Figure 18. Sensitivity tests are carried out by varying the temperature- and pressure-dependence of the exponential model. For the Arrhenius model, van den Berg et al. (2010) used a viscosity prefactor of 4.98×10^{17} . In this study we search the viscosity prefactor that would result in the same viscosity average as the uniform viscosity used in model A2 and A4 (Section 4.3.2). The differences produced by the different choice of viscosity scale factor in the Arrhenius model is also illustrated in Figure 18.

Equations are as follows:

Arrhenius viscosity model

$$\eta_{Arr}(P, T) = B \exp\left(\frac{E^* + PV^*}{RT}\right) \quad (11)$$

where T and P are dimensional temperature and pressure values.

Exponential viscosity model

$$\eta_{exp}(T, z) = \eta_0 \exp(cz - bT) \quad (12)$$

where T and P are non-dimensional, $b = \ln \Delta\eta_T$, $c = \ln \Delta\eta_P$

Viscosity decreases with Temperature and increases with pressure. As we can see from Figure 18, the viscosity profile is shifted left to lower values when temperature dependence is increase in the exponential model. When the depth dependence is increased, the viscosity profile shifts to higher values at depth, while remaining the same on the surface. The Arrhenius model shows a similar trend, but its depth-dependence is in general higher.

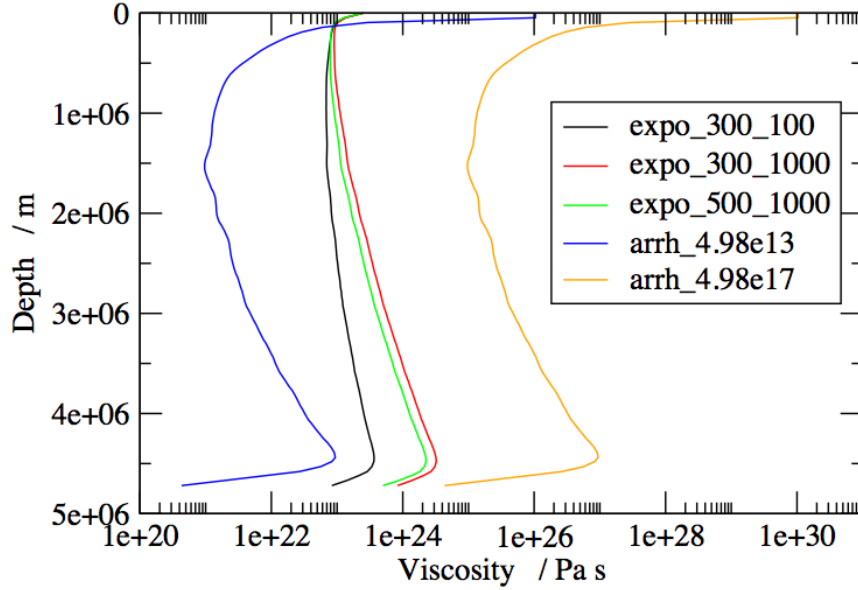


Figure 18: Depth-dependent viscosity profiles. *expo* and *arrh* in the legend denote the exponential viscosity model and the Arrhenius model, respectively. For exponential models, $\Delta\eta_T$ and $\Delta\eta_P$ are listed. For Arrhenius models, the viscosity prefactor is indicated.

Parameter	Description	Value	Unit
B	Viscosity prefactor	4.98×10^{13}	Pa s
E^*	Activation energy	3×10^5	J/mol
V^*	Activation volume	0.5×10^{-6}	m ³ /mol
R	Gas constant	8.3144	J K ⁻¹ mol ⁻¹
η_0	Viscosity scale value	2.5×10^{23}	Pa s
$\Delta\eta_T$	Layer viscosity contrast due to T	-	-
$\Delta\eta_P$	Layer viscosity contrast due to P	-	-

Table 7: Parameters used in dynamical models with Earth-like core mass fraction.

B The density, adiabatic temperature, and solidus profiles of core-less dynamical models

A Fortran program is developed to investigate the radial density, adiabatic temperature, and solidus distributions in the interior of a spherically symmetric core-less super-Earth planet. This program is modified from program sources of the Geodynamics course (van den Berg, 2011). The density profile is approximated iteratively based on a pressure-dependent compressibility model on an equidistant grid of 500 nodal points. Incompressibility (K) is parameterised in terms of density in Equation 15. This parameterisation corresponds to a linear increase of incompressibility with depth, similar to the Murnaghan 1st order equation of state (Poirier, 1991). Corresponding values of K and K' are taken from post perovskite properties and applied in the calculations. Gravity and pressure profiles are integrated according to the density profile and in turn used to update the density profile using a trapezium approximation to the integration formula (Equation 16). A uniform density profile is used as the initial profile. Density, gravity, and pressure profiles are updated iteratively until a convergence is achieved in the density profile. The convergence is defined such that the total root mean square of differences at each nodal point between the last density profile and the previous one is smaller than 0.01 % of the average density.

Based on such incompressible density calculations, the total mass of core-less super-Earths are calculated for a range of radii values. The results are presented in Figure (to be inserted). A radius is particularly searched for $8 M_{\oplus}$, and is found to be 13459 km. Temperature profiles are integrated along adiabatic gradients according to Equation 17. Due to the extended Bussenesq formulation, the volume average density of calculated profiles is prescribed as the uniform density in dynamical models. This density is 4679.3 kg/m^3 , which would correspond to a compressibility factor of $f = 0.849$ (Section 3.2). Accordingly, a linear gravity profile is used in the dynamical models, with zero value at the planet's centre.

$$\rho(r) = \rho_0 \exp \left(\int_r^R \frac{\rho(r')}{K(r')} g(r') dr' \right) \quad (13)$$

$$g(r') = \frac{Gm(r)}{r'^2}, \quad m(r) = \int_0^r \rho(r') 4\pi r'^2 dr' \quad (14)$$

$$K = C\rho^n, \quad n = K'_0 \quad (15)$$

$$\rho_i^{(j+1)} = \rho_{i+1}^{(j+1)} \exp \left(\frac{1}{2} \Delta r \left(\frac{\rho_{i+1}^{(j)} g_{i+1}^{(j)}}{K_{i+1}^{(j)}} + \frac{\rho_i^{(j)} g_i^{(j)}}{K_i^{(j)}} \right) \right), \quad i = N - 1, \dots, 1 \quad (16)$$

$$\left(\frac{\partial T}{\partial r} \right)_S = \frac{T\alpha g}{c_p} \quad (17)$$

A solidus is calculated based on the experimental results and extrapolation method used in Zerr et al. (1998). Melting temperatures are measured in materials of a pyrolite type of composition, representing the lower mantle, up to 59 GPa. The solidus is extrapolated with a pressure-dependent Gruneisen parameter, based on the observed parallel trend of the magnesiowüstite melting curve and that of pyrolite (Zerr et al, 1998). A Lindemann melting law is fitted to the data (Equation 18;

Zerr and Boehler, 1994), where γ is the thermal Grüneisen parameter. The Grüneisen parameter is parameterised in a power-law relation with the density (Equation 19; Boehler and Ramakrishnan, 1980). The surface Grüneisen parameter is taken as 1.3. The melting temperature of lower mantle material is taken as 2800 K at 660 km depth (Boehler, 2000). This is taken as the starting point of the interpolation. The Grüneisen is calculated based on the density profile (Equation 13) calculated above. The calculated melting curve for the coreless model agrees with the solidus temperature measurement (4300 ± 270 K) of olivine at around CMB (135 GPa) conditions (Holland and Ahrens, 1997), which is expected to break down to a perovskite-magnesiowüstite assemblage. The melting temperature for depths above 660 km is simply back interpolated using the same relations.

$$\frac{d \ln T_m}{d \ln \rho} = 2 \left(\gamma - \frac{1}{3} \right) \quad (18)$$

$$\frac{\gamma}{\gamma_0} = \left(\frac{\rho_0}{\rho} \right)^{1.3} \quad (19)$$